Experimental investigation of the creep behavior of MgO at high pressures

Shenghua Mei and David L. Kohlstedt *University of Minnesota, 310 Pillsbury Dr. SE, Minneapolis, MN 55455*

William B. Durham *Massachusetts Institute of Technology, 77 Massachusetts Ave., Cambridge, MA 02129*

Liping Wang *Stony Brook University, John S. Toll Road, Stony Brook, NY 11794*

Abstract. The high-temperature rheological behavior of polycrystalline periclase, MgO, has been investigated using the deformation-DIA on a synchrotron beamline at pressures up to 10 GPa. Significant experimental scatter in stress measurement illustrates current limitations of this technique. Although temperature and stress sensitivities are not well constrained, there is a clear dependence of creep rate on pressure. Based on our results, the creep rate of MgO depends on confining pressure with an activation volume of $V^* \approx 3.7 \times 10^{-6}$ m^3/mol. The grain-scale view of deformation processes reveals, as other D-DIA studies have, that subpopulations of grains, grouped by orientation, obey slightly different flow laws. The measurements also reveal that stress heterogeneity in the sample, whether caused by external conditions or processes internal to the sample itself, contribute a significant portion of the overall uncertainty in stress measurement.

1. Introduction

The deformation behavior of MgO has long received attention in both materials science and geosciences. In the former, a wide range of applications of MgO in industry demand a thorough understanding of its mechanical behavior [e.g., *Copley and Pask,* 1965a; 1965b; *Gorum et al*., 1960]. In the latter, the creep behavior of MgO has been investigated, for example, by *Weaver and Paterson* [1969], *Paterson and Weaver* [1970], *Meade and Jeanloz* [1988], and *Sinogeikin and Bass* [1999] in order to understand geodynamic processes occurring within Earth's interior, from deep-focus earthquakes to

mantle convection. Although the emphasis as well as experimental conditions might be different, both kinds of studies share not only the same trunk but also many of the same branches.

A distinct feature of studies carried out in geosciences is the high-pressure environment since pressure is a critical thermodynamic parameter in describing any physical process occurring deep within Earth's interior. *Paterson and Weaver* [1970] conducted deformation experiments on polycrystalline MgO at temperatures from 25^{o} to 750^{o}C at pressures up to 0.5 GPa using a gas-medium press; they quantified mainly the deformation behavior of MgO in the transition from the brittle to the ductile regime. Recently, *Merkel et. al.* [2002] used a diamond anvil cell to deform MgO at room temperature at pressures up to 47 GPa; they focused on investigating texture development within specimens with increasing pressure.

The dependence of creep behavior of MgO on pressure at high temperatures has yet to be investigated, severely limiting our understanding of geological processes based on laboratory studies. To further define the high-temperature, high-pressure creep behavior of MgO, we have conducted a series of experiments using a deformation-DIA (D-DIA) apparatus at a synchrotron beamline. We have explored the rheological properties of our MgO samples at temperatures up to 1573 K and pressures up to 10 GPa. The focus of this study is quantification of the creep behavior of MgO at high temperatures and high pressures in order to provide a basis for applying flow laws obtained in the laboratory to processes occurring within Earth's interior.

2. Experimental Details

2.1. Sample assembly and experiments

Experiments were carried out in the D-DIA apparatus [*Wang, et al.*, 2002] at the National Synchrotron Light Source (NSLS), Brookhaven National Laboratory. Though technical features on conducting such deformation experiments with using D-DIA have been illustrated elsewhere [*Li, et al.*, 2004, *Chen, et al.*, 2006], a few details relevant especially to this study are briefly elaborated here for clarity.

Each sample is assembled within a 6-mm edge length cubic pressure medium of either boron-epoxy resin or mullite. In general, experiments conducted in this study are aimed at quantifying creep behavior of two different minerals: olivine and MgO. Specifically, a cold-pressed MgO sample (0.8 mm length x 1.1 mm diameter) and a hot-pressed olivine sample (1.1 mm length x 1.1 mm diameter) were assembled with Al_2O_3 pistons, a boron nitride sleeve, and a graphite resistance heater into the cubic pressure medium. Nickel discs located at the ends of the samples acted as strain makers, since most of the assembly parts are x-ray transparent. A sketch of the sample assembly is presented in Figure 1. The temperature during the experiments was either measured directly using a W3%Re-W25%Re thermocouple embedded in one of the Al_2O_3 pistons or was estimated based on calibrated heater power vs. temperature curves in assemblies prepared without a thermocouple.

At the start of an experiment, the cell was first pressurized hydrostatically to the desired level, heated to run temperature, and then the sample deformed in triaxial compression at constant pressure. Deformation resulted from pushing top and bottom anvils toward each other. During an experiment, a beam of white x rays (50x50 μm in size) passed through deforming sample, and diffraction patterns as well as x radiographs of the deformation column were taken every ~15 min. This information is used, as described next, in computing pressure, differential stress, and strain for each run.

2.2. Data acquisition and processing

Strain. In the synchrotron beamline, x radiographs taken every ~15 min of the sample column are used to measure the change in length of a sample during a deformation experiment. A radiograph of a typical deforming sample is shown in Figure 2. Such images make it possible to measure the change in sample length to within a few microns. A typical length vs. elapsed time plot is shown in Figure 3.

Pressure and differential stress. The state of elastic lattice strain in the sample is determined via x-ray diffraction measurements, and the state of stress is calculated based on non-isotropic elastic lattice strains within the sample [*Singh*, 1993; *Singh, et al.*, 1998; *Weidner, et al.*, 1994; *Weidner, et al.*, 1998]. The four elements of the solid-state x-ray

detector system are oriented such that diffracted x rays from (*hkl*) planes whose normals lie either nearly parallel to (vertical in lab coordinates) or nearly perpendicular to (horizontal) the applied stress axis are detected simultaneously. We thus refer to the four elements as "vertical" and "horizontal" detectors. Diffraction patterns collected simultaneously on detectors aligned parallel to the compression axis (vertical detectors) and perpendicular to the compression axis (horizontal detectors) are compared in Figure 4 for a sample of MgO. If we call d_V the spacing of planes whose Bragg reflections are detected by the vertical detectors and d_H detected the horizontal detectors, then the *d*-spacing corresponding to the mean stress (i.e., mean pressure *P*) is

$$d_P = (d_V + 2d_H)/3. \quad (1)$$

Based on the analysis of *d*-spacings described above, mean stress as well as the differential stress can be computed.

For a specific lattice plane (*hkl*), *P* was deduced from unit-cell volume and a 3rd order Birch-Murnaghan EOS [Birch, 1947; Murnaghan, 1937] given as

$$V = [d_P(h^2 + k^2 + l^2)^{1/2}]^3 \quad (2)$$

and

$$P = \frac{K(T)}{K'}[(V_0(T)/V)^{K'} - 1] \quad (3)$$

where K is the bulk modulus, K' =dK/dP, and V_0 is the unit-cell volume at room pressure. Both K and V_0 are function of T. More details of these parameters are given elsewhere [*Speziale, et al.*, 2001; *Zha, et al.*, 2000].

Differential stress within a deforming sample can be computed from the product of the elastic moduli and the non-isotropic elastic lattice strains. For present purposes, we compute differential stresses using *Singh*'s [1998] formulation assuming that the material is in the iso-stress (*Reuss*) state, although it is now widely recognized that a polycrystalline material that has yielded plastically is typically not in the *Reuss* state [*Li*

et al., 2004; *Weidner, et al.*, 2004; *Merkel*, 2006]. The differential stress (σ) in the *Reuss* state is

$$\sigma = 2G_R(d_H - d_V)/d_P \tag{4}$$

where G_R is the aggregate shear modulus for the cubic system derived from the compliance S_{ij} as

$$G_R = \frac{1}{2}[S_{11} - S_{12} - 3(S_{11} - S_{12} - \tfrac{1}{2}S_{44})\Gamma_{hkl}]^{-1} \tag{5}$$

with

$$\Gamma_{hkl} = (h^2k^2 + k^2l^2 + l^2h^2)/(h^2 + k^2 + l^2)^2 \tag{6}$$

Typical results for pressure and differential stress vs. elapsed time for a deformation experiment are illustrated in Figure 5.

Crystalline materials, including MgO, typically exhibit plastic anisotropy, meaning that the flow stress (akin to σ in Eq. 7) depends on the orientation of the crystallographic axes relative to the deviatoric stress tensor. For a polycrystalline material with grains randomly oriented, not all grains yield at the same differential stress. The result is that local stresses begin to redistribute from the moment of plastic yield, so that whole solid departs, often in a very short amount of strain, from the *Reuss* state [*Chen, et al.*, 2006; *Merkel and Yagi*, 2006; *Weidner and Li*, 2006; *Weidner, et al.*, 2004]. *Singh et al*. [1998] suggest a compromise formulation wherein the effective shear modulus lies between G_R and that appropriate to the iso-strain (*Voigt*) state G_V, computed as $\alpha[2G_R(hkl)]^{-1} + (1-\alpha)(2G_v)^{-1}$. However, during plastic flow, one often observes a non-physical value of $\alpha > 1$ (e.g., *Chen et al*. [2006]). Efforts are currently underway to apply numerical methods to turn the complexity of information revealed by x-ray diffraction to simple forms of the rheological law. As stated above, for present purposes of identifying the effect of pressure on the flow of polycrystalline MgO, we give results calculated using Equation (4).

3. Results and Discussion

Five samples of polycrystalline MgO were tested in the D-DIA at constant displacement rates ranging from 1.4 to 6.5 × 10^{-5} s^{-1} over true axial strains of 17 to 41% at temperatures of 1350 to 1573 K and pressures of 1.45 to 10 GPa. Two of the experiments consisted of multiple temperature steps, with deformation halted between steps. Although the stress measurements were rather noisy, as will be seen shortly, after a brief initial transient, they did not exhibit clear strain hardening or strain weakening; thus, we characterized each deformation step with a single value of differential stress. Results are listed in Table 1. Creep curve from one run that involved temperature stepping are shown in Figure 5. For most of the runs, we were able to discern with confidence diffraction peaks only at the MgO (111) and (200) reflections; for runs san68 and san69, we were also able to measure peaks for (222) and (400). Differential stresses $\sigma(hkl)$ in Table 1 are given for only the two strongest reflections.

Measurement uncertainties are significant and a serious concern to us. Absolute temperatures are known to roughly ±50 to ±75 K in the hot zone along the length of the sample, which is a typical pathology of development work (such as this) involving small sample volumes and cell configurations that are altered slightly run to run (as ours are) in search of an ideal design. Uncertainties in differential stress are even more substantial. Understanding the causes of stress uncertainty is a subject of ongoing development by our group and others; an analysis of the problem, except for some observations reported below regarding stress heterogeneity, is beyond the scope of this paper. For the present, we call stress uncertainty the range of stress covering a loosely defined "substantial portion" of observed scatter. The (200) reflection invariably produces the strongest peak; over the course of 3-4 measurements of a deformation step, the stress uncertainty is roughly ±0.04 GPa. The (111) reflection, whose diffraction peak has a much lower intensity, the uncertainty is typically ±0.15 GPa (Figure 5). Comparably, the uncertainty in measured pressure is small, on the order of ~10%.

MgO can be easily deformed at high temperatures by crystalline slip since both of its sets of slip systems, {110}<110> and {001}<110>, become active when T >873 K, thus providing five independent slip systems required by the *von Mises-Taylor* criterion for homogeneous crystalline ductility [*Copley and Pask*, 1965a; *Paterson and Weaver*, 1970]. We therefore analyze our results in terms of a power law equation of the form

$$\dot{\varepsilon}(\sigma, T, P) = A\sigma^n \exp\left(-\frac{Q + PV^*}{RT}\right) \quad (7)$$

where $\dot{\varepsilon}$ is axial strain rate, σ is differential stress, T is temperature, P is confining pressure. Our objective is to identify the four material parameters: A, the pre-exponential; n, the stress exponent; Q, the activation energy; and V^*, the activation volume.

The narrow range of experimental strain rates combined with measurement noise does not allow reasonable constraint on the values of all four of these parameters. We therefore assert that $n = 3$, a reasonable value for high-temperature dislocation glide or climb-controlled dislocation creep of MgO [*Wilshire*, 1995], and then fit the data from the (200) reflection to obtain the values for A, Q, and V^* that are reported in Table 2. The best fit for activation volume with $n = 3$ is ~3.7×10^{-6} m^3/mol for each reflection. This value is in good agreement with that reported for diffusion of oxygen in MgO by *Van Orman et al.* [2003]. It agrees also with that for deformation estimated by *Weidner et al*. [1994] of 4-7×10^{-6} m^3/mol obtained by comparing their results on the high pressure strength of MgO to that of *Hulse et al.* [1963] at lower pressures.

The final results are presented in Figure 6 as a semi-log plot of differential stress vs. pressure, normalized to a common temperature and strain rate using the best fit parameters (Table 2) and Equation (7). The total uncertainty in stress (i.e., the scatter as described above) and temperature has been combined into a single error bar for each point by using Equation (7) to convert temperature to an equivalent stress. Despite the magnitude of the overall uncertainty, the positive trend of differential stress with pressure is visible. Stress measurements based on the (111) reflection are much less precise than those obtained from the (200) reflection. Nonetheless, the dependence of stress on

pressure obtained from the (111) reflection is qualitatively similar to that determined using the (200) reflection.

Stresses determined from the (111) reflection are about two times higher than those obtained from the (200) reflection. Therefore, given the geometric relationship between x-ray detectors and applied stress, we can conclude that under current conditions the stress applied normal to (111) planes experiences significantly higher resistance to deformation than does the stress applied normal to (100) planes. In terms of the known slip systems in MgO, this observation is consistent with the observation that the {001}<110> slip systems are harder than the {110}<110> slip systems at the conditions of these experiments [*Weaver and Paterson*, 1969].

The best fit value for the activation energy of $Q = 47$ kJ/mol is much lower than those expected for creep mechanisms involving self-diffusion, which are usually above 200 kJ/mol [*Frost and Ashby*, 1982]. However, $Q = 200$ kJ/mol, while not the best fit value, is not badly inconsistent with our data and still results in a somewhat smaller best fit value of V^* (Table 2). Since lower values of n will also fit our data, we cannot at this point rule out the possibility of creep by a grain-size sensitive mechanism such as grain boundary sliding accommodated by a dislocation creep process, which typical yield $n \leq 2$ [e.g., *Langdon*, 1994].

As noted above, values obtained for differential stress are generally scattered, yet values of stress determined from parallel (e.g., (200) and (400)) lattice reflections appear to be reasonably well correlated. In the current configuration, diffraction peaks other than (111) and (200) were too weak to measure except in runs san68 and san69. Stress measurements on two pairs of parallel reflections – (200) vs. (400) and (111) vs. (222) – are plotted in Figure 5 for San68. The correlation between (200) and (400) is quite clear; all but 1 of the 12 pairs of points are within 0.1 GPa of one another, while the range of scatter was estimated above to be 0.08 GPa (i.e., ± 0.04 GPa). For the pair of reflections (111) and (222), the scatter of individual reflections is 0.3 GPa (±0.15 GPa), with only 4 of the 12 pairs of points differing by more than this amount. Determinations of stress from parallel sets of reflections are independent measurements of the state of the same

volume of material at the same moment in time. Discrepancies between measurements must owe their existence to uncertainties introduced by the measurement system (geometry of sample, beam, collimator, and detectors, as well as details associated with the multi-channel analyzer and peak-fitting software). Therefore, in Figure 6, we infer that a substantial portion of the scatter in the values of stress determined from a single reflection ((200) or (111)) results from physical changes to the diffracted volume between measurements. Temperature fluctuations have a small effect on elastic constant of MgO [*Spetzler*, 1970] and thus may account for some of the scatter in Figure 6. Temperature fluctuations also directly affect the strength of a sample, and temperature gradients give rise to spatial gradients in strength. In addition, the differential stress will vary spatially within the sample due to the finite strength of the solid confining medium. In addition, due to the relatively small length-to-diameter ratio of a sample, a relatively large dead zone develops due to friction between the sample and the pistons. The volume sampled by the x-rays undoubtedly changes from one exposure to the next due to dynamic effects that occur during deformation and due to slight shifts in the position of the sample with respect to the x-ray beam.

4. Conclusions

These experiments mark some of the first attempts to carry out high-strain compressional deformation experiments in a D-DIA apparatus. Significant uncertainties in the values of stress and of temperature impair our ability to measure flow parameters with sufficient accuracy to discern flow mechanism. Nevertheless, the measurements indicate a positive pressure dependence of the flow stress with $V^* \approx 3.7\times10^{-6}$ m^3/mol. This work involves not only the development of a piece of hardware, the D-DIA, but also the formulation of an approach to handling a new type of input to deformation science, namely, the measurement of stress and strain rate at the grain scale. As has been observed previously in similar experiments on plastic flow of polycrystalline samples, a grain scale redistribution of differential stress occurs among different orientation populations of grains. Interpretation of the different flow laws obtained from analysis of different sets of diffraction peaks is a topic of ongoing study. We also see with rather good resolution that, apart from the stress redistribution just mentioned, the stress distribution is spatially

significantly non-uniform within a sample. This observation is quite independent of the system (e.g., slits, collimators, and detectors) that measures the intensities of diffracted x-rays. It is not clear at this point if the cause is extrinsic (i.e., imposed by non-uniform tractions on the outer surfaces of the sample from pistons and pressure medium) or if it is inherent to deformation processes within the polycrystalline sample itself.

Acknowledgments:

This research was supported by the U.S. Department of Energy, Office of Basic Energy Sciences under contract W-7405-ENG-48 (LLNL) and grant DE-FG02-04ER15500 (UMN). Experiments were carried out at the X17B2 beamline of the National Synchrotron Light Source, which is supported by the U.S. Department of Energy, Division of Materials Sciences and Division of Chemical Sciences under Contract No. DE-AC02-76CH00016 and by COMPRES, the Consortium for Materials Properties Research in Earth Sciences under NSF Cooperative Agreement EAR 01-35554. We thank Drs Mike Vaughan, Donald Weidner, Li Li for their technical support and/or discussions at the X17B2 beamline.

References

Birch, F, 1947. Finite elastic strain of cubic crystals. *Phys Rev.*, 71: 809-824.

Chen, J.H., Li, L., Yu, T., Long, H., Weidner, D., Wang, L., and Vaughan, M., 2006. Do Reuss and Voigt bounds really bound in high-pressure rheology experiments? *J. Phys: Condens. Matter*, 18: 1049-59.

Copley, S. M., and Pask, J. A., 1965a. Deformation of polycrystalline MgO at elevated temperatures. *J. Am. Ceram. Soc.*, 48: 636-41.

Copley, S. M., and Pask, J. A., 1965b. Plastic deformation of MgO single crystals up to 1600 ^{o}C. *J. Am. Ceram. Soc.*, 48: 139-46.

Frost, H.J., and Ashby, M.F., 1982. *Deformation Mechanism Maps*, 167 pp. Pergamon, New York.

Gorum, A.E., Luhman, W. J., and Pask, J. A., 1960. Effect of impurities and heat-treatment on ductility of MgO. *J. Am. Ceram. Soc*., 43: 241-45.

Hulse, C. O., Copley, S. M., and Pask, J. A., 1963. Effect of crystal orientation on plastic deformation of magnesium oxide. *J. Amer. Ceram. Soc.*, 46: 317-323.

Langdon, T. G., 1994. A unified approach to grain boundary sliding in creep and superplasticity. *Acta Metall.* 42: 2437-2443.

Li, L., Weidner, D. J., Chen, J. H., Vaughan, M., Davis, M., and Durham, W. B., 2004. X-ray strain analysis at high pressure: Effect of plastic deformation in MgO. *J. Appl. Phys.*, 95, 12: 8357-8365.

Li, L., Weidner, D., Raterron, P., Chen, J. H., and Vaughan, M., 2004. Stress measurements of deforming olivine at high pressure. *Phys. Earth Planet. Inter.* 143/144: 357-67.

Meade, C., and Jeanloz, R., 1988. Yield strength of MgO to 40 GPa. *J. Geophys. Res.* B93: 3261–9.

Merkel, S., Wenk, H. R., Shu, J., Shen, G., Gillet, P., Mao, H. K., and Hemley, R. J., 2002. Deformation of polycrystalline MgO at pressures of the lower mantle. *J. Geophys. Res.*, 107: 2271 (doi: 10. 1029/2001JB000920).

Merkel, S., 2006, X-ray diffraction evaluation of stress in high pressure deformation experiments. *Journal of Physics-Condensed Matter*, 18: S949-S962.

Merkel, S., and Yagi, T., 2006. Effect of lattice preferred orientation on lattice strains in polycrystalline materials deformed under high pressure: Application to hcp-Co. *Journal of Physics and Chemistry of Solids*, 67: 2119-2131.

Murnaghan, F. D., 1937. Finite deformations of an elastic solid. *Am J Math.*, 49: 235-260.

Paterson, M. S., and Weaver, C. W., 1970. Deformation of polycrystalline MgO under pressure. *J. Am. Ceram. Soc.*, 53: 463-72.

Singh, A. K., 1993. The lattice strain in a specimen (cubic system) compressed nonhydrostatically in an opposed anvil device. *J. Appl. Phys.*, 73: 4278-86.

Singh, A. K., Balasingh, C., Mao, H-K., Hemley, R. J., and Shu, J., 1998. Analysis of lattice strains measured under nonhydrostatic pressure. *J. Appl. Phys.*, 83: 7567-75.

Sinogeikin, S.V., and Bass, J. D., 1999. Single-crystal elasticity of MgO at high pressure. *Phys. Rev.*, B 59: 14141-4.

Spetzler, H., 1970. Equation of state of polycrystalline and single-crystal MgO to 8 kilobars and 800 K. *J. Geophys. Res.*, 75: 2073-2087.

Speziale, S., Zha, C. S., Duffy, T. S., Hemley, R. J., and Mao, H. K., 2001. Quasi-hydrostatic compression of magnesium oxide to 52 GPa: Implications for the pressure-volume-temperature equation of state. *J. Geophys. Res.*, 106: 515–528.

Van Orman, J. A., Fei, Y., Hauri, E. H., and Wang, J., 2003. Diffusion in MgO at high pressures: Constraints on deformation mechanisms and chemical transport at the core-mantle boundary. *Geophy. Res. Lett.*, 30, 2: 1056, (doi:10.1029/2002GL016343).

Wang, Y. B., Durham, W. B., Getting, I. C., and Weidner, D. J., 2003. The deformation-DIA: a new apparatus for high temperature triaxial deformation to pressures up to 15 GPa. *Rev. Sci. Instrum.*, 74: 3002-11.

Weaver, C. W., and Paterson, M. S., 1969. Deformation of cube-oriented MgO crystals under pressure. *J. Am. Ceram. Soc.*, 52: 293-302.

Weidner, D. J., Li, L., Wang, Y., and Vaughan, M. T., 1994. Yeild strength at high pressure and temperature. *Geophys. Res. Lett.*, 21, 9: 753-56.

Weidner, D. J., Wang, Y., Chen, G., Ando, J., and Vaughan, M. T., 1998. Rheology measurements at high pressure and temperature. *Properties of Earth and Planetary Materials at High Pressure and Temperature (Geophysical Monograph)*, v101, pp 473–82.

Weidner, D. J., Li, L., Davis, M., and Chen, J. H., 2004. Effect of plasticity on elastic modulus measurements. *Geophys. Res. Lett.*, 31, L06621 (doi: 10. 1029/2003 GL019090).

Weidner, D. J., and Li, L., 2006. Measurement of stress using synchrotron x-rays. *Journal of Physics-Condensed Matter*, 18: S1061-S1067.

Wilshire, B. 1995. Creep mechanisms in single and polycrystalline MgO. *Brit. Ceram. Trans.* 94: 57-63.

Zha, C. S., Mao, H. K., and Hemley, R. J., 2000. Elasticity of MgO and a primary pressure scale to 55 GPa. Proc. Natl. Acad. Sci. U.S.A., 97, 13:494 –13,499.

Table 1. Experimental conditions and results.

Exp	P, GPa	Strain rate, s^{-1}	T, K	ε	$\sigma(111)$, MPa	$\sigma(200)$, MPa
67	3.1	2.5×10^{-5}	1373	0.27	300	133
68(1)	2.4	3.0×10^{-5}	1373	0.35	380	168
68(2)	2.2	3.1×10^{-5}	1473	0.20	300	149
68(3)	1.45	3.2×10^{-5}	1573	0.17	160	96
69(1)	5.2	3.1×10^{-5}	1373	0.36	300	138
69(2)	4.4	4.2×10^{-5}	1473	0.29	--	204
69(3)	4	6.5×10^{-5}	1573	0.41	320	168
76	10	4.0×10^{-5}	1350	0.38	520	550
96	8.8	1.4×10^{-5}	1373	0.32	300	149

Table 2. Best fit parameters for (200) reflection to Equation (7).

	$n \equiv 3$	$n \equiv 3$ $Q \equiv 200$ kJ/mol
$\log A$	-8.84	-3.55
n	≡3	≡3
Q, kJ/mol	47	≡200
V^*, $\times 10^{-6}$ m^3/mol	3.7	2.0

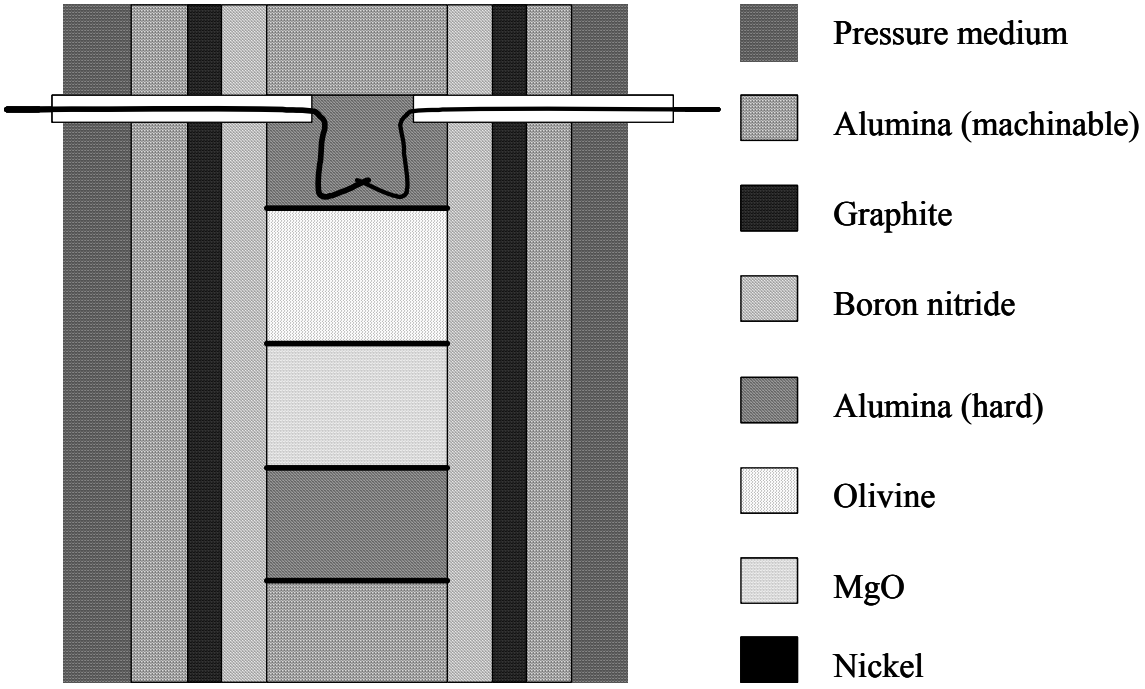

Figure 1. Sketch of sample assembly. Samples (MgO and olivine) were assembled with hard alumina pistons, machinable alumina plugs, a boron nitride sleeve, a graphite resistance heater, and a machinable alumina sleeve into a 6-mm edge length cubic pressure medium. Nickel discs were placed between neighboring pieces in the sample column as strain makers. The temperature during an experiment was in general measured using a W3%Re-W25%Re thermocouple embedded in one of the alumina pistons. Deformation of the olivine is the subject of another study (manuscript in preparation).

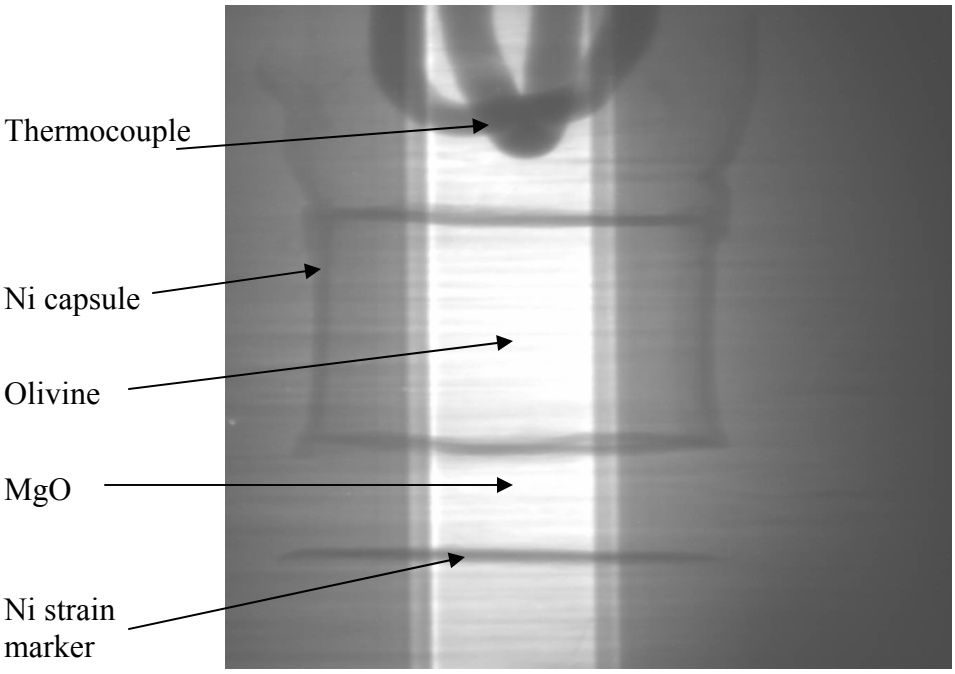

Figure 2. Radiograph of sample column as taken periodically during deformation, viewed through the transparent anvils of the D-DIA. The lighter vertical stripe is a portion of the sample column exposed in the gap between anvils. Nickel disks are placed between column pieces as strain markers. The nickel capsule surrounding the olivine sample

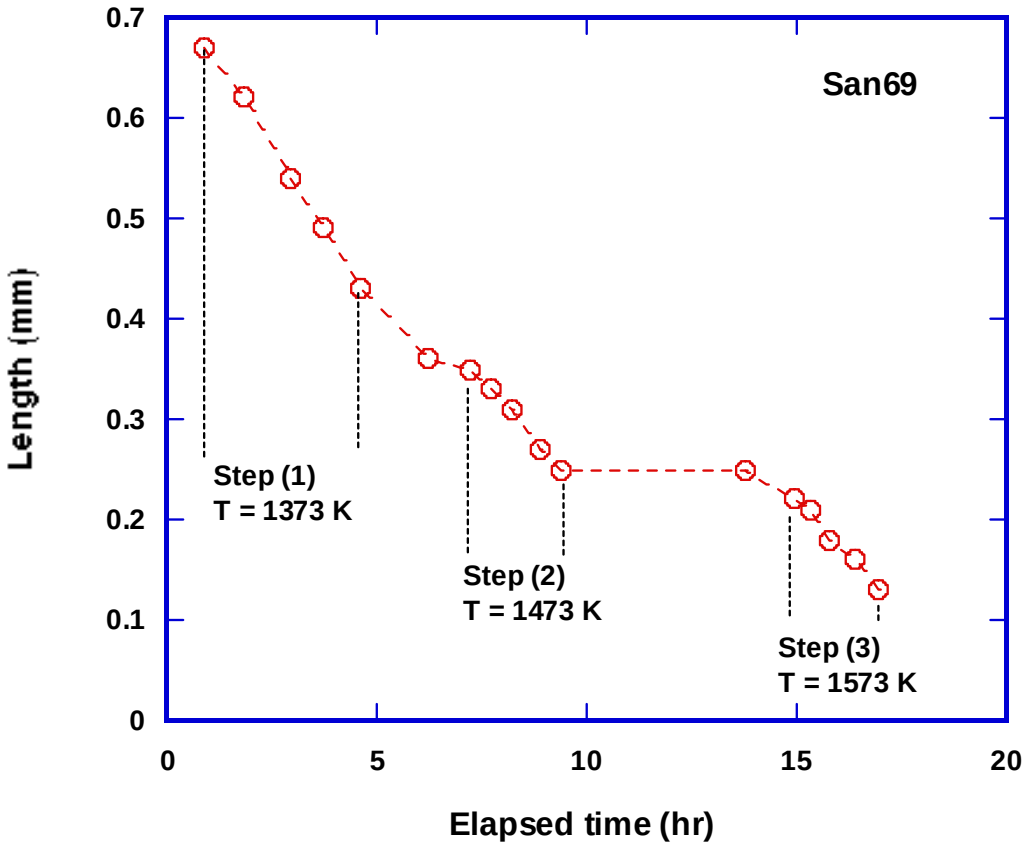

Figure 3. Typical plot of sample length vs. elapsed time from a deformation experiment on one sample. In general, a run involves several steps including a change in temperature at a fixed pressure or a change in pressure at a given temperature.

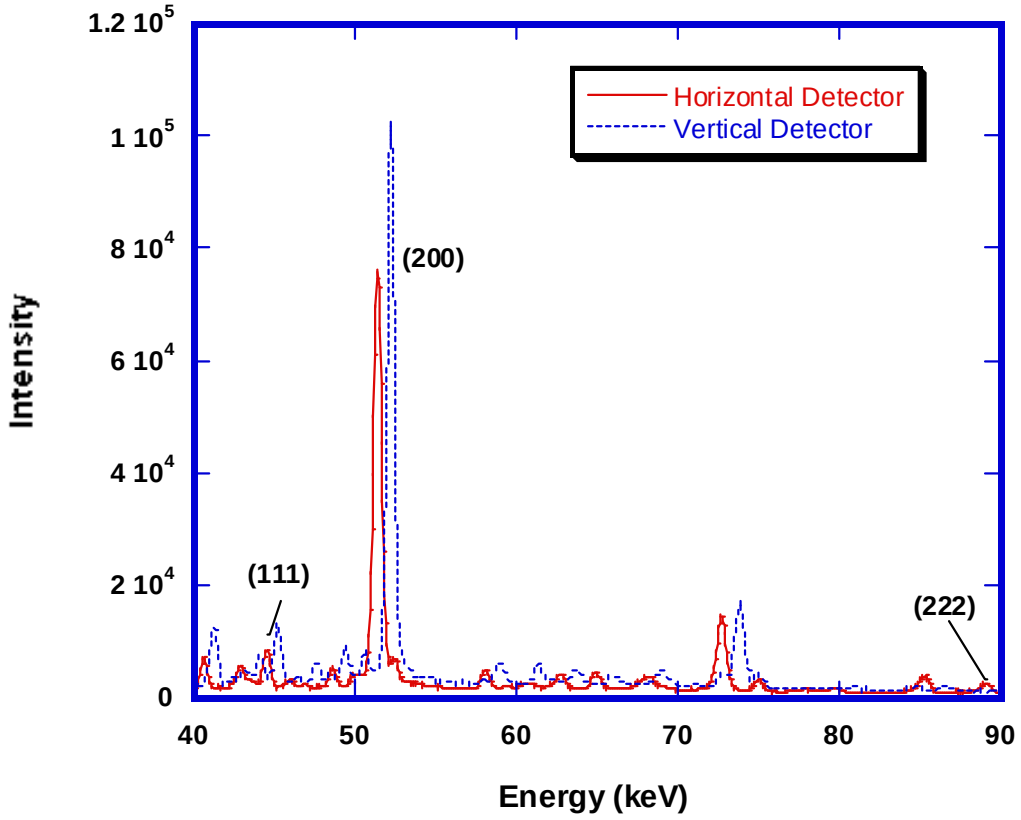

Figure 4. Typical diffraction patterns from MgO collected simultaneously on the detectors aligned parallel to the compression axis (vertical detectors) and perpendicular to the compressionl axis (horizontal detectors). For both, $2\theta = 6.8^{o}$. The relative shift of diffraction peaks between vertical and horizontal detectors is a measure of the differential stress applied to the specimen.

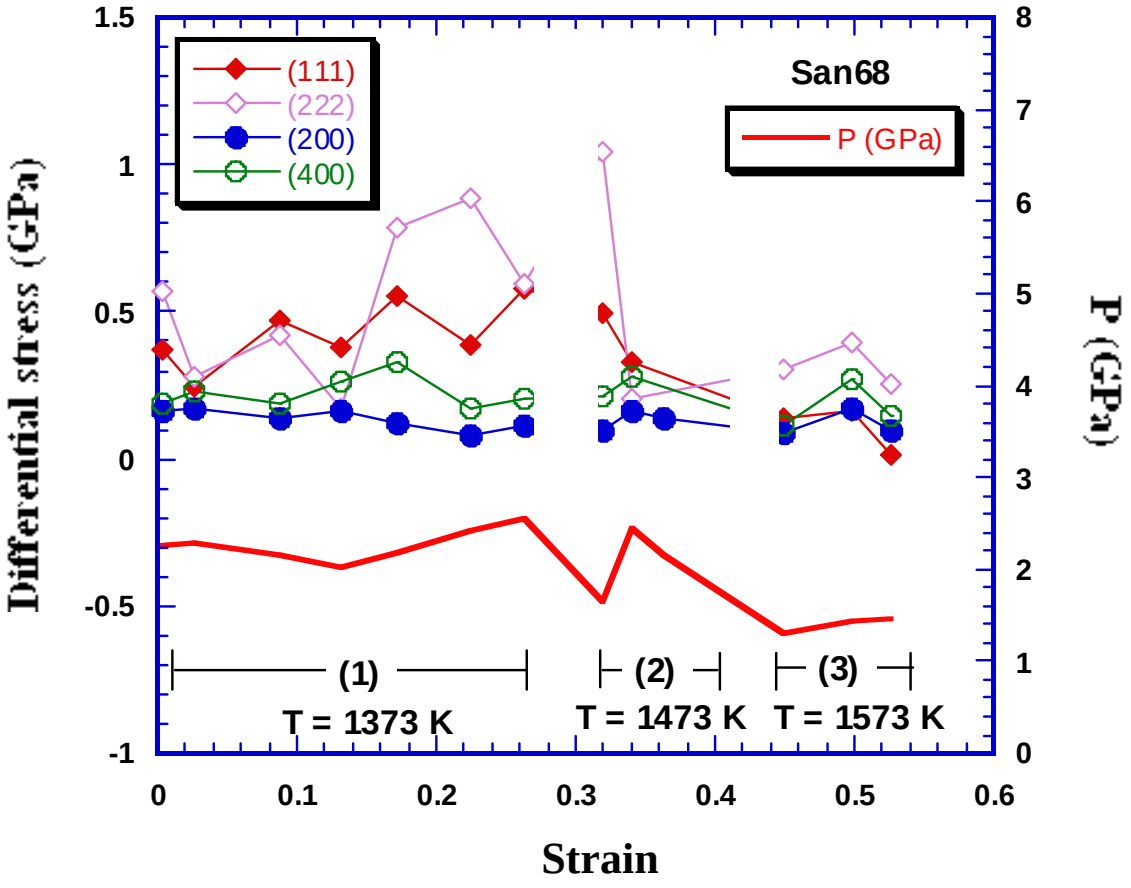

Figure 5. Differential stress and pressure vs. strain for run san68. Differential stresses were determined from four different (*hkl*) reflections as shown. Three separate deformation steps were taken on sample, labeled (1) – (3). Between each step deformation was stopped, temperature raised to the new value, and deformation restarted.

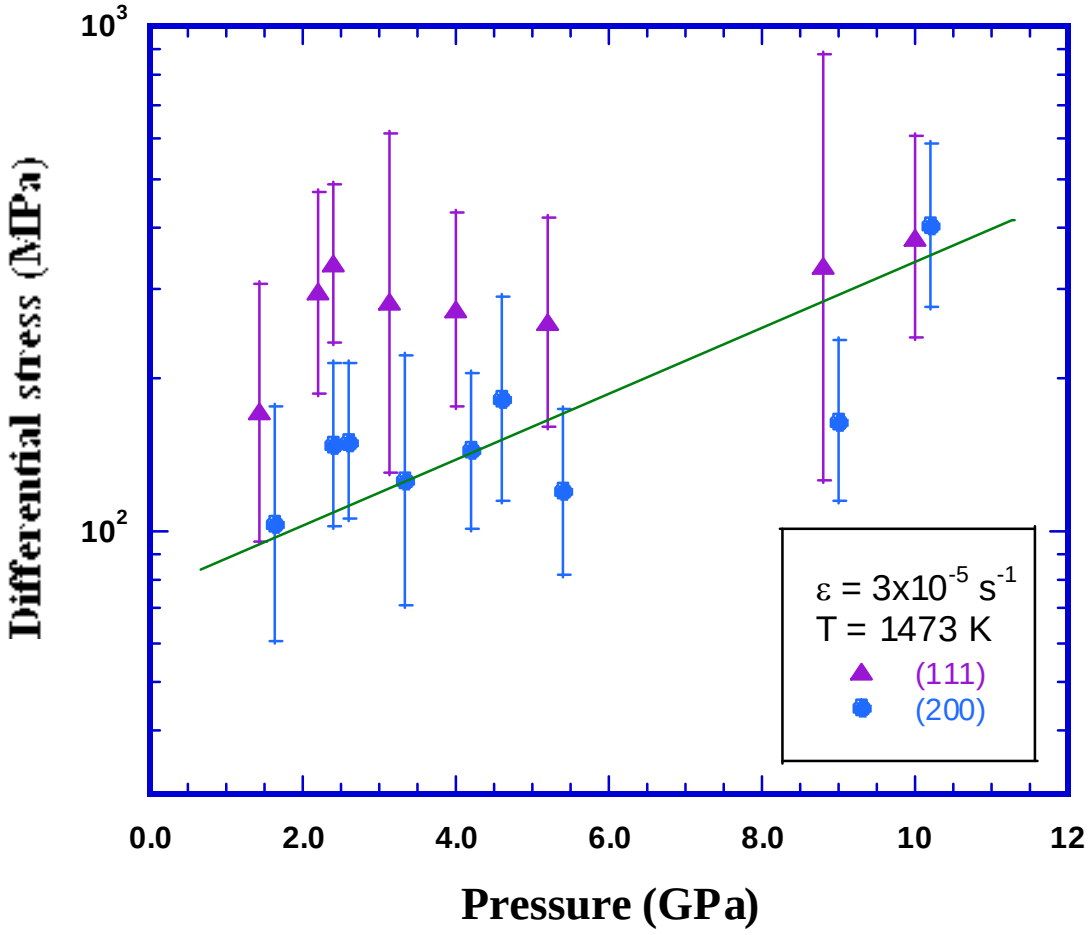

Figure 6. Semi-log plot of differential stress vs. confining pressure based on 9 deformation steps on 5 samples based on measurements made with the two most prominent Bragg reflections in MgO, (111) and (200). Actual temperatures and strain rates are given in Table 1; for plotting purposes, stresses have been normalized to 1473 K and 3×10^{-5} s^{-1} using Equation (7) and the flow parameters in Table 2. The straight line is the least-squares best fit to the (200) data with *n* constrained to 3. The uncertainties, especially for the (111) measurements, are substantial (also illustrated in Figure 5), yet a positive dependence of differential stress on pressure is discernable.